

# Correlations between Low-Frequency QPOs and Spectral Parameters in XTE J1550–564 and GRO J1655–40

Gregory J. Sobczak

Astronomy Dept., Harvard University, 60 Garden St., Cambridge, MA 02138;  
gsobczak@cfa.harvard.edu

Jeffrey E. McClintock

Harvard-Smithsonian Center for Astrophysics, 60 Garden St., Cambridge, MA 02138;  
jem@cfa.harvard.edu

Ronald A. Remillard, Wei Cui, Alan M. Levine, and Edward H. Morgan  
Center for Space Research, MIT, Cambridge, MA 02139; rr@space.mit.edu,  
cui@space.mit.edu, aml@space.mit.edu, ehm@space.mit.edu

Jerome A. Orosz

Sterrekundig Instituut, Universiteit Utrecht, Postbus 80.000, 3508 TA Utrecht, The  
Netherlands; J.A.Orosz@astro.uu.nl

Charles D. Bailyn

Department of Astronomy, Yale University, P. O. Box 208101, New Haven, CT 06520;  
bailyn@astro.yale.edu

Received \_\_\_\_\_; accepted \_\_\_\_\_

## ABSTRACT

Utilizing observations obtained with the *Rossi X-ray Timing Explorer*, we examine correlations between the properties of 0.08–22 Hz variable frequency QPOs and the X-ray spectral parameters for the black hole candidates XTE J1550–564 and GRO J1655–40. The spectra were fitted to a model including a multi-temperature blackbody disk and a power-law component. We find that the QPO frequency and amplitude are well correlated with the spectral parameters, although the correlations found for XTE J1550–564 are generally opposite to those for GRO J1655–40. There is one exception: Both sources exhibit a general increase in the QPO frequency as the disk flux increases (or as the mass accretion rate through the disk increases). In addition, these QPOs are observed only when the power-law component contributes more than 20% of the 2–20 keV flux, which indicates that both the disk and the power-law components are linked to the QPO phenomenon.

*Subject headings:* black hole physics — stars: individual (XTE J1550-564) — stars: individual (GRO J1655–40) — X-rays: stars

## 1. Introduction

GRO J1655–40 is a black hole X-ray nova (BHXN) with a dynamically-determined primary mass of  $\sim 7 M_{\odot}$  (Orosz & Bailyn 1997; Shahbaz et al. 1999), which exceeds the maximum mass of a neutron star (Rhoades & Ruffini 1974; Kalogera & Baym 1996). The source displays superluminal radio jets and is at a distance of  $3.2 \pm 0.2$  kpc (Hjellming & Rupen 1995). GRO J1655–40 was discovered with BATSE on 1994 July 27, and in early 1996 it entered a very low or quiescent state. However, a second outburst commenced on 1996 April 25 and continued for 16 months. During this second outburst, there was an intensive campaign of observations with the *Rossi X-ray Timing Explorer* (RXTE); this paper is based on extensive spectral and timing results derived from these 52 1996-97 observations (Sobczak et al. 1999a; Remillard et al. 1999a; see also Mendez et al. 1998).

XTE J1550–564 is an X-ray nova (aka soft X-ray transient) and a black hole candidate, which was discovered on 1998 September 6 (Smith et al. 1998). Two weeks later it reached a peak intensity of 6.8 Crab at 2–10 keV to become the brightest X-ray nova yet observed with RXTE. The source has been observed in the very high, high/soft, and intermediate canonical outburst states of BHXN (Sobczak et al. 1999bc; Cui et al. 1999). There is both a radio counterpart (Campbell-Wilson et al. 1998) and an optical counterpart, which has been studied extensively in outburst (Jain et al. 1999; Sanchez-Fernandez et al. 1999). The mass of the compact primary is unknown. The data presented herein are based on 169 pointed observations with RXTE, which represent all of the pointed observations of XTE J1550–564 during Gain Epoch 3 (i.e. before 16:30 (UT) on 1999 March 22).

Both GRO J1655–40 and XTE J1550–564 are of intense current interest because they display a variety quasi-periodic X-ray oscillations (QPOs) which can be used to probe the accretion process around black holes. It is well known that the temporal characteristics of black hole candidates are strongly correlated with the spectral state (see van der Klis 1995,

and references therein). QPOs are fundamental properties of the accretion flow and in a few sources the rms amplitude can exceed 15% of the mean X-ray flux (see §4). Consequently, simultaneous studies of the temporal and spectral properties of BHXN are a promising avenue for determining the origin of QPOs in these sources.

GRO J1655–40 exhibits four types of QPOs between 0.1 Hz and 300 Hz (Remillard et al. 1999a), three of which have relatively stable central frequencies. A fourth QPO with a central frequency that varies from 14–22 Hz is the only one of interest here. Similarly, the power spectra of XTE J1550–564 exhibit two types of QPOs: a high-frequency QPO ( $\sim 200$  Hz) and a variable 0.08–18 Hz QPO (Remillard et al. 1999b; Sobczak et al. 1999b; Cui et al. 1999). Again, we are interested only in this latter QPO. Our focus in this paper is on the correlations between the frequency and amplitude of the 0.08–18 Hz and 14–22 Hz QPOs and the spectral parameters for these two sources. We explore the implications of these correlations for the origin of these QPOs and compare our results with several QPO models.

## 2. Observations and Analysis

The timing and spectral data were obtained using the Proportional Counter Array (PCA; Jahoda et al. 1996) onboard the *Rossi X-ray Timing Explorer* (RXTE). The PCA consists of five xenon-filled detector units (PCUs) with a total effective area of  $\sim 6200$  cm<sup>2</sup> at 5 keV. The PCA is sensitive in the range 2–60 keV, the energy resolution is  $\sim 17\%$  at 5 keV, and the time resolution capability is 1  $\mu$ sec.

The PCA spectral data in the energy range 2.5–20 keV were fit to the widely used model consisting of a multi-temperature blackbody accretion disk plus power-law (Tanaka & Lewin 1995, and references therein). The spectral parameters include the temperature

and radius of the inner accretion disk and the power-law photon index; the power-law flux and the disk flux were derived from the fitted parameters. See Sobczak et al. (1999abc) for additional information regarding spectral fitting methods. The fitted temperature and radius of the inner accretion disk presented here are the observed color temperature and radius of the inner disk. Since the disk emission is likely to be affected by spectral hardening due to electron scattering (Shakura & Sunyaev 1973), the physical interpretation of these parameters remains uncertain.

An X-ray timing analysis was conducted by computing the 2–30 keV power spectrum for each PCA observation. The contribution from counting statistical noise was subtracted and the power spectra were corrected for dead-time effects as described by Zhang et al. (1995) and Morgan, Remillard, & Greiner (1997). A chi-squared minimization technique was used to derive the central frequency and width of each QPO. The QPO features were fit with Lorentzian functions, while the power continuum in the vicinity of the QPO feature was modeled with a power-law function. Triple QPO features exhibiting a fundamental as well as sub- and first-harmonics were common (see Fig. 1a). We identify the central QPO feature with the largest rms amplitude as the fundamental. The integrated fractional rms amplitude of the QPO is the square root of the integrated power in the QPO feature, expressed as a fraction of the mean count rate. The amplitudes of weaker QPOs at harmonic frequencies have been excluded from the QPO amplitude discussed here. See Remillard et al. (1999ab) and for further information regarding the timing analysis of the data for GRO J1655–40 and XTE J1550–564. QPOs observed during the rising phase of XTE J1550–564 (observations 1–14 in Table 1) were first reported by Cui et al. (1999) and details of the timing analysis for those observations can be found therein.

For GRO J1655–40, we consider RXTE programs 10255 and 20402, which constitute almost all of the RXTE exposures of this source. Spectral parameters for GRO J1655–40

are given in Table 1 of Sobczak et al. (1999a) and the QPO parameters are given in Table 3 of Remillard et al. (1999a). The observations of XTE J1550–564 include exposures under RXTE programs 30188-06, 30191, 30435, and 40401, with spectral parameters published in Table 1 of Sobczak et al. (1999bc) and QPO parameters listed here in Table 1.

For four observations listed in Table 1, more than one QPO frequency is given (observations 153–154 & 166–167). In these cases, the QPOs are of approximately equal amplitude and are blended together. Consequently, we are unable to identify the fundamental component, and we have excluded these data from the figures presented here. The QPO frequencies of observations 15–75 listed in Table 1 differ slightly from the corresponding entries (1–60) in Table 1 of Sobczak et al. (1999b), because we used the improved fitting technique described above.

### 3. Results

We now investigate the correlations between the frequency/amplitude of the QPOs and the X-ray spectral parameters of GRO J1655–40 and XTE J1550–564. As noted above, our interest is focused on the strong QPOs in the range 0.08–22 Hz that routinely exhibit changes in frequency from day to day. The correlations between QPO frequency and the spectral parameters are shown in Figures 2 & 3 and the correlations between QPO amplitude and the spectral parameters are shown in Figures 4 & 5. The open circles in Figures 2–7 represent those observations in which high-frequency (161–300 Hz) QPOs are also present.

For both sources, the variable QPO frequency is correlated with all of the spectral parameters plotted in Figures 2a–2f & 3a–3f with a few exceptions (e.g. the vertical branch with  $\nu > 17$  Hz in Fig. 2d). However, the respective correlations for the two sources are

generally in the opposite sense, although there is a slight similarity between the QPO frequency vs.  $T_{in}$  relation for both sources. The only striking exception to the contrary correlations between QPO frequency and the spectral parameters for the two sources is the relation between QPO frequency and disk flux shown in Figures 2c & 2f. In this case, QPO frequency is correlated with the temperature and inner disk radius of the disk in such a way that both sources exhibit a general increase in the QPO frequency as the disk flux increases. This relation for XTE J1550–564 appears roughly linear in the range 1–7 Hz if one excludes the observations when high-frequency QPOs are present (open circles in Fig. 2c).

The QPO amplitude is generally not well correlated with the spectral parameters for both sources (Fig. 4a–4f & 5a–5f), and these correlations are more complicated than the ones considered above. For XTE J1550–564, the QPO amplitude is not well correlated with the temperature or radius of the inner disk (Fig. 4a & 4b), but the QPO amplitude does generally decrease as the disk flux increases (Fig. 4c). Also for XTE J1550–564, the QPO amplitude is correlated with the photon index for  $\Gamma = 1.5 - 2.1$ , but not well correlated for  $\Gamma > 2.1$  (Fig. 5a). In the case of GRO J1655–40, the correlations exhibit two branches, with high-frequency QPOs present on one branch and absent on the other (Fig. 4d–4f & Fig. 5d–5f). For GRO J1655–40, note that the branch without high-frequency QPOs consistently has the steeper slope. The correlations involving the photon index, power-law flux, and total flux for XTE J1550–564 also exhibit two- or possibly three-branches (Fig. 5a–5c). However, the branches are less distinct and the high-frequency QPOs are not restricted to a single branch.

The correlations between QPO amplitude and QPO frequency are shown in Figure 6a–6b for both sources. The QPO amplitude generally decreases as the frequency increases for both sources. The QPO amplitude for XTE J1550–564 is very high and typically about an order of magnitude greater than the amplitude for GRO J1655–40. On the other hand,

the QPO frequency is about twice as high on average for GRO J1655–40. The black hole candidate GRS 1915+105 displays QPOs in approximately the same frequency range and with approximately the same amplitude as XTE J1550–564. The correlations between QPO frequency and amplitude and the spectral parameters for GRS 1915+105 are similar to those of XTE J1550–564 (Muno, Morgan, & Remillard 1999). The larger amplitudes and lower frequencies of the QPOs in XTE J1550–564 and GRS 1915+105 may indicate that the QPO mechanism in these two sources is operating in a different regime than for GRO J1655–40 (due to differences in the mass accretion rate or central mass) or that a different QPO mechanism is at work.

#### 4. Discussion

Both XTE J1550–564 and GRO J1655–40 exhibit a similar, strong positive correlation between the QPO frequency and disk flux in X-rays. A similar quasi-linear relation between these two quantities was found for the variable 1–15 Hz QPOs in GRS 1915+105 (Markwardt, Swank, & Taam 1999) and the 20–30 Hz QPOs in XTE J1748–288 (Revnivtsev, Trudolyubov, & Borozdon 1999). The correlation between QPO frequency and disk flux suggests that the QPO frequency is intimately related to the accretion disk. Since the contribution of the disk to the total flux in XTE J1550–564 and GRO J1655–40 varies from 5–95% (Sobczak et al. 1999abc), the disk flux is not necessarily a good indicator of the total mass accretion rate. However, the disk flux alone is a reasonable measure of the mass accretion rate through the inner disk. *Therefore, we can conclude that the QPO frequency increases as the mass accretion rate through the inner disk increases.*

The QPOs are also related to the power-law component: The variable frequency QPOs appear in XTE J1550–564 and GRO J1655–40 only when the power-law contributes more than 20% of the 2–20 keV flux (Sobczak et al. 1999abc). Figure 7 shows the power-law



flux vs. the disk flux. There is a clear distinction in the observations with and without QPOs: The observations *without* QPOs cluster in a nearly horizontal line at low power-law flux (Fig. 7b,d), whereas the observations *with* QPOs show significant vertical displacements toward increased power-law flux (Fig. 7ac). The same distinction between observations with and without QPOs is present in GRS 1915+105 (Muno et al. 1999). *We conclude that not only is the QPO frequency tied to the accretion disk (see above), but in addition the QPO phenomenon is closely related to the power-law component: The power-law flux must reach a threshold of  $\sim 20\%$  of the 2–20 keV flux to trigger the QPO mechanism.*

The variable frequency QPOs in GRO J1655–40 and XTE J1550–564 generally yield rms amplitudes in the range of 0.3–1.5% and 1–15% of the mean count rate, respectively. The X-ray luminosity of XTE J1550–564, which is  $\sim 2 \times 10^{38} (D/6\text{kpc})^2 \text{ erg s}^{-1}$  at typical brightness levels ( $\sim 2$  Crab) when QPOs are seen, is modulated with a crest-to-trough ratio as high as 1.5 (see Fig. 1b). Previously, only the microquasar GRS1915+105 has shown QPOs with such a large amplitude and a high luminosity (Morgan et al. 1997). The large modulation of the X-ray luminosity indicates that these QPOs originate within several gravitational radii ( $r_g = GM/c^2$ ) of the central object where most of the gravitational energy is liberated in the accretion flow. The QPO frequency cannot be the Keplerian frequency at these radii without some novel mechanism for transporting energy out to large radii, because a 10 Hz QPO would correspond to a radius of 700 km (or  $\sim 50 r_g$ ) for a  $10 M_\odot$  black hole.

As discussed by Markwardt et al. (1999), neither the beat frequency model (Alpar & Shaham 1985) nor the sonic point model (Miller, Lamb, & Psaltis 1998) are applicable to the  $\sim 10$  Hz variable frequency QPOs observed in BHCs. Thermal-viscous instabilities (Chen & Taam 1994; Abramowicz, Chen & Taam 1995) can produce strong oscillations; however, their 0.02–0.06 Hz frequencies are well below most of the 0.08–22 Hz QPOs discussed here.

Moreover, this model predicts a negative rather than a positive correlation between the QPO frequency and mass accretion rate. One model that does predict large-amplitude QPOs near 10 Hz, which are positively correlated with the mass accretion rate, invokes an oscillating shock near the inner disk (Molteni, Sponholtz, & Chakrabarti 1996). However, it is not clear whether such a shock is present for accretion flows with high specific angular momentum (Narayan, Kato, & Honma 1997).

Another possibility is that the variable frequency QPOs are the result of radiation-driven oscillations in a quasi-spherical accretion flow or corona (Cui 1999). Fortner, Lamb, & Miller (1989) modeled radiation-driven radial oscillations for neutron stars with luminosities near the Eddington luminosity. The oscillation frequency is dominated by the inflow time from the outer part of the radial flow, which corresponds to  $\sim 10$  Hz if the radial flow begins a few hundred km from the central object. The observed increase in the QPO frequency as the mass accretion rate through the disk increases could be caused by a shrinking of the radial inflow region. However, in simulations by Fortner et al. (1989), the luminosity is modulated by only  $\sim 1\%$  compared to the almost 15% modulation observed for XTE J1550–564.

## 5. Conclusions

For XTE J1550–564 and GRO J1655–40, the QPO frequency and amplitude are correlated at some level with all of the spectral parameters, as illustrated in Figures 2–5. However, in the case of the QPO frequency, the correlations are generally opposite for the two sources. The only exception is the QPO frequency vs. disk flux plotted in Figures 2c & 2f. *Both sources exhibit a general increase in the QPO frequency as the disk flux increases.* The correlation between QPO frequency and disk flux suggests that the QPO frequency is intimately related to the accretion disk. The same relation was found for variable 1–15 Hz

QPOs in GRS 1915+105 (Markwardt et al. 1999) and 20–30 Hz QPOs in XTE J1748–288 (Revnivtsev et al. 1999). Since the disk flux is a reasonable measure of the mass accretion rate through the disk, we can conclude that the QPO frequency increases as the mass accretion rate through the disk increases. In addition, the QPOs are present only when the power-law contributes more than 20% of the 2–20 keV flux, which indicates that both the disk and the power-law components are linked to the QPO phenomenon. The QPO amplitude for XTE J1550–564 is very high and typically about an order of magnitude greater than the amplitude for GRO J1655–40, whereas the QPO frequency is about twice as high for GRO J1655–40. This behavior may indicate that the QPO mechanism is operating in a different regime for each source, which may relate to why the correlations are generally opposite for the two sources.

The correlations between the QPO frequency and amplitude and the X-ray spectral parameters demonstrate that the QPO phenomenon is linked to the overall emission properties of the source. No current model for the origin of these QPOs can adequately explain more than a few of the many correlations presented here. We hope that this study will inspire further significant theoretical work on the subject.

This work was supported, in part, by NASA grant NAG5-3680 and the NASA contract to MIT for instruments of RXTE. Partial support for J.M. and G.S. was provided by the Smithsonian Institution Scholarly Studies Program. W.C. would like to thank Shuang Nan Zhang and Wan Chen for extensive discussions on spectral modeling and interpretation of the results.

## REFERENCES

- Abramowicz, M. A., Chen, X., & Taam, R. E. 1995, *ApJ*, 452, 379
- Alpar, M. A. & Shaham, J. 1985, *Nature*, 316, 239
- Campbell-Wilson, D., McIntyre, V., Hunstead, R., & Green, A. 1998, *IAU Circ.* 7010
- Chen, X. & Taam, R. E. 1995, *ApJ*, 441, 354
- Cui, W. 1999, Proc. “High Energy Processes in Accreting Black Holes”, Eds. J. Poutanen & R. Svensson (ASP: San Francisco), ASP Conf. Ser. Vol. 161, p. 97
- Cui, W., Zhang, S. N., Chen, W., & Morgan, E. H. 1999, *ApJ*, 512, L43
- Ebisawa, K., Ogawa, M., Aoki, T., Dotani, T., Takizawa, M., Tanaka, Y., Yoshida, K., Miyamoto, S., Iga, S., Hayashida, K., Kitamoto, S., & Terada, K. 1994, *PASJ*, 46, 375
- Fortner, B., Lamb, F. K., & Miller, G. S. 1989, *Nature*, 342, 775
- Hjellming, R. M. & Rupen, M. P. 1995, *Nature*, 375, 464
- Jahoda, K., Swank, J. H., Giles, A. B., Stark, M. J., Strohmayer, T., Zhang, W., & Morgan, E. H. 1996, Proc. SPIE 2808, “EUV and Gamma Ray Instrumentation for Astronomy” VII, 59
- Jain, R., Bailyn, C. D., Orosz, J. A., Remillard R. A., & McClintock, J. E. 1999, *ApJ*, 517, L131
- Kalogera, V. & Baym, G. 1996, *ApJ*, 470, L61
- Makishima, K., Maejima, Y., Mitsuda, K., Bradt, H. V., Remillard, R. A., Tuohy, I. R., Hoshi, R., & Nakagawa, M. 1986, *ApJ*, 308, 635
- Markwardt, C. B., Swank, J. H., & Taam, R. E. 1999, *ApJ*, 513, L37

- McClintock, J. E. 1998, in *Accretion Processes in Astrophysical Systems*, ed. S. S. Holt & T. Kallman (Woodbury, NY: AIP), 290
- Mendez, M., Belloni, T., & van der Klis, M. 1998, *ApJ*, 499, L187
- Miller, M. C., Lamb, F. K., & Psaltis, D. 1998, *ApJ*, 508, 791
- Mitsuda, K., et al. 1984, *PASJ*, 36, 741
- Molteni, D., Sponholz, H., & Chakrabarti, S. K. 1996, *ApJ*, 457, 805
- Morgan, E. H., Remillard, R. A. & Greiner, J. 1997, *ApJ*, 482, 993
- Muno, M. P., Morgan, E. H., & Remillard, R. A. 1999, *ApJ*, submitted, astro-ph/9904087
- Narayan, R., Kato, S., & Honma, F. 1997, *ApJ*, 476, 49
- Orosz, J. A. & Bailyn, C. D. 1997, *ApJ*, 477, 876
- Remillard, R. A., Morgan, E. H., McClintock, J. E., Bailyn, C. D., & Orosz, J. A. 1999a, *ApJ*, 522, 397
- Remillard, R. A., McClintock, J. E., Sobczak, G. J., Bailyn, C. D., Orosz, J. A., Morgan, E. H., & Levine, A. M. 1999b, *ApJ*, 517, L127
- Revnivtsev, M. G., Trudolyubov, & Borozdin, K. N. 1999, astro-ph/9903306
- Rhoades, C. E. & Ruffini, R. 1974, *Phys. Rev. Lett.*, 32, 324
- Sanchez-Fernandez, C. et al. 1999, *A&A*, 348, L9
- Shahbaz, T., van der Hooft, F., Casares, J., Charles, P. A., & van Paradijs, J. 1999, *MNRAS*, 306, 89
- Shakura, N. I. & Sunyaev, R. A. 1973, *A&A*, 24, 337
- Shimura, T. & Takahara, F. 1995, *ApJ*, 445, 780
- Smith, D. A. & RXTE/ASM teams 1998, *IAU Circ.* 7008

- Sobczak, G. J., McClintock, J. E., Remillard, R. A., Bailyn, C. D., & Orosz, J. A. 1999a, *ApJ*, 520, 776
- Sobczak, G. J., McClintock, J. E., Remillard, R. A., Levine, A. M., Morgan, E. H., Bailyn, C. D., & Orosz, J. A. 1999b, *ApJ*, 517, L121
- Sobczak, G. J., McClintock, J. E., Remillard, R. A., Cui, W., Levine, A. M., Morgan, E. H., Orosz, J. A. & Bailyn, C. D. 1999c, in preparation
- Tanaka, Y. & Lewin, W. H. G. 1995, in *X-ray Binaries*, ed. W. H. G. Lewin, J. van Paradijs, & E. P. J. van den Heuvel (Cambridge: Cambridge Univ. Press), p. 126
- van der Klis, M. 1995, in *X-ray Binaries*, ed. W. H. G. Lewin, J. van Paradijs, & E. P. J. van den Heuvel (Cambridge: Cambridge Univ. Press), p. 252
- Zhang, W., Jahoda, K., Swank, J. H., Morgan, E. H., & Giles, A. B., 1995, 449, 930

Table 1. QPO Parameters for XTE J1550–564<sup>†</sup>

Obs #	Date (yymmdd)	MJD <sup>a</sup>	QPO Freq. <sup>b</sup> (Hz)	QPO Amp. <sup>c</sup> (% rms)	Q <sup>d</sup>
1	980907	51063.70	0.084	13.9±1.5	59.7
2	980908	51064.01	0.12	14.2±0.6	6.7
3	980909	51065.07	0.29	14.3±0.7	14.1
4	980909	51065.34	0.39	15.0±0.5	9.4
5	980910	51066.07	0.81	15.7±0.4	8.4
6	980910	51066.34	1.0	15.6±0.4	9.4
7	980911	51067.27	1.6	16.1±0.4	8.3
8	980912	51068.35	2.4	14.3±0.2	11.9
9	980913	51069.27	3.4	12.9±0.2	11.4
10	980914	51070.13	3.2	13.1±0.2	12.8
11	980914	51070.27	3.2	13.0±0.2	12.9
12	980915	51071.20	3.7	13.0±0.2	13.8
13	980915	51072.00	2.6	11.6±0.8	22.9
14	980916	51072.34	4.0	12.9±0.2	15.5
15	980918	51074.14	5.7	9.4±0.3	8.6
16	980919	51075.99	13.1 <sup>e</sup>	1.05±0.05	2.8
17	980920	51076.80	7.2 <sup>e</sup>	6.6±0.1	5.0
18	980920	51076.95	8.5 <sup>e</sup>	4.8±0.1	4.3
19	980921	51077.14	9.8	3.3±0.1	9.2
20	980921	51077.21	7.0	4.0±0.1	5.4
21	980921	51077.87	5.8	4.8±0.2	11.6
22	980922	51078.13	5.4	10.0±0.2	10.7
23	980923	51079.79	4.2	12.9±0.4	7.4
24	980924	51080.08	3.9	12.2±0.4	13.6
25	980925	51081.06	2.9	13.4±0.4	9.8
26	980926	51082.00	2.7	14.0±0.4	10.4
27	980927	51083.00	2.6	14.4±0.4	8.9
28	980928	51084.34	2.7	14.1±0.5	11.0
29	980929	51085.27	4.1	12.6±0.3	11.1
30	980929	51085.92	2.9	14.3±0.6	9.5
31	980929	51085.99	3.0	14.4±0.6	6.5
32	980930	51086.89	3.5	14.0±0.2	8.2
33	981001	51087.72	3.4	14.2±0.3	8.9
34	981002	51088.01	3.2	14.4±0.4	8.6
35	981003	51089.01	3.0	15.0±0.5	8.2

Table 1—Continued

Obs #	Date (yymmdd)	MJD <sup>a</sup>	QPO Freq. <sup>b</sup> (Hz)	QPO Amp. <sup>c</sup> (% rms)	Q <sup>d</sup>
36	981004	51090.14	3.9	13.3±0.4	10.2
37	981004	51090.70	3.7	13.7±0.4	9.5
38	981005	51091.74	5.6	10.0±0.3	11.4
39	981007	51093.14	6.5	7.5±0.3	11.1
40	981008	51094.14	4.3	12.4±0.4	11.1
41	981008	51094.57	5.1	11.3±0.3	11.2
42	981009	51095.61	4.5	12.1±0.6	12.8
43	981010	51096.57	5.5	11.7±0.2	4.9
44	981011	51097.57	4.7	12.0±0.5	10.3
45	981011	51097.81	4.2	13.5±0.6	9.9
46	981012	51098.28	5.0	11.6±0.4	10.1
47	981013	51099.22	4.8	11.5±0.5	11.1
48	981013	51099.61	5.0	11.7±0.3	9.0
49	981014	51100.29	6.5	7.6±0.3	10.9
50	981015	51101.61	6.8	7.0±0.3	6.7
51	981015	51101.94	6.7	7.0±0.3	9.1
52	981020	51106.95	5.5 <sup>e</sup>	3.8±0.1	8.9
53	981022	51108.08	5.4 <sup>e</sup>	4.1±0.0	8.7
54	981023	51109.74	4.9 <sup>e</sup>	4.0±0.1	11.2
59	981029	51115.28	6.8 <sup>e</sup>	2.8±0.2	1.8
64	981109	51126.59	4.9	2.7±0.2	1.9
151	990302	51239.08	18.1	0.52±0.06	17.6
153	990304	51241.83	5.9/10.3±0.2 <sup>e</sup>	2.9±0.1/2.8±0.1	3.0/1.6
154	990305	51242.51	5.7/10.0±0.3 <sup>e</sup>	2.4±0.1/2.8±0.2	2.5/1.4
155	990307	51244.50	8.4±0.3 <sup>e</sup>	1.5±0.2	1.8
156	990308	51245.35	6.4 <sup>e</sup>	3.6±0.1	11.7
157	990309	51246.41	7.9±0.2 <sup>e</sup>	1.8±0.1	1.3
158	990310	51247.98	6.1 <sup>e</sup>	3.7±0.1	9.9
159	990311	51248.09	5.9 <sup>e</sup>	3.7±0.1	11.0
160	990312	51249.40	6.2 <sup>e</sup>	3.8±0.1	9.4
161	990313	51250.69	6.7	6.5±0.3	8.8
162	990316	51253.23	5.5 <sup>e</sup>	4.3±0.1	9.6
163	990317	51254.09	6.1 <sup>e</sup>	3.8±0.1	3.4
164	990318	51255.09	6.2 <sup>e</sup>	2.4±0.2	1.9
166	990321	51258.09	5.2/9.1±0.9 <sup>e</sup>	2.6±0.4/2.8±0.6	3.0/1.5



Table 1—Continued

Obs #	Date (yymmdd)	MJD <sup>a</sup>	QPO Freq. <sup>b</sup> (Hz)	QPO Amp. <sup>c</sup> (% rms)	Q <sup>d</sup>
167	990321	51258.50	5.5/10.1±0.3 <sup>e</sup>	2.5±0.2/2.6±0.3	2.4/2.2
177 <sup>f</sup>	990401	51269.68	4.5±0.2	1.5±0.4	3.7
178 <sup>f</sup>	990402	51270.74	8.9 <sup>e</sup>	2.9±0.2	3.5
179 <sup>f</sup>	990403	51271.41	9.1 <sup>e</sup>	2.8±0.2	4.8

<sup>†</sup>209 PCA observations are given in Sobczak et al. (1999c), but only those observations that exhibit QPOs are listed in this table.

<sup>a</sup>Start of observation,  $MJD = JD - 2,400,000.5$ .

<sup>b</sup>Errors are given at the 95% confidence level. The statistical errors in the QPO centroid frequency are  $< 1\%$ , unless given otherwise.

<sup>c</sup>Errors are given at the 95% confidence level.

<sup>d</sup>Q = Centroid/FWHM

<sup>e</sup>Indicates observations during which high frequency (161–283 Hz) QPOs are also observed.

<sup>f</sup>PCA Gain Epoch 4 – The spectral information for these observations is not as reliable as that obtained for PCA Gain Epoch 3; therefore, the Epoch 4 data is not included in the figures presented here.

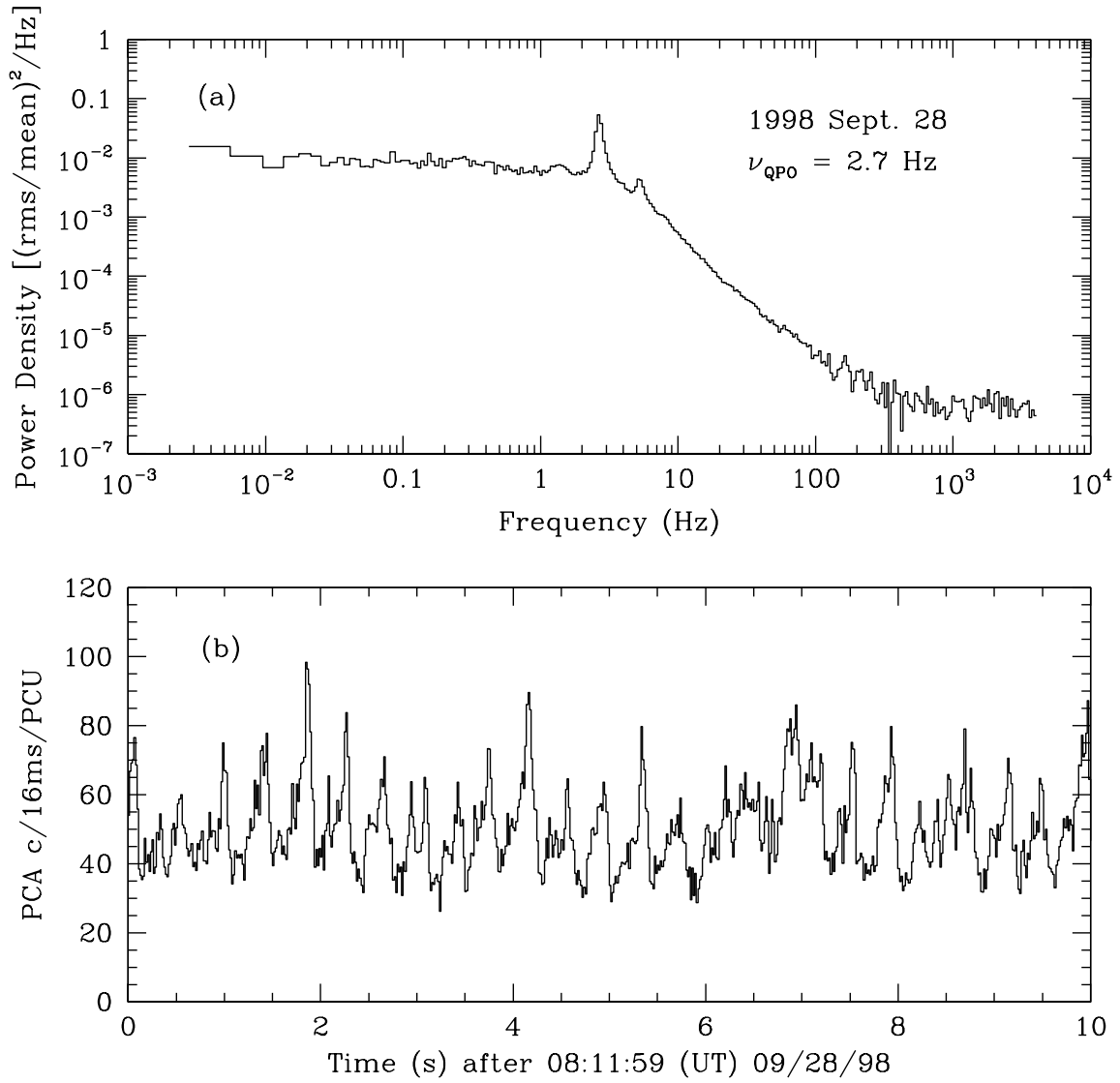


Fig. 1.— Sample power density spectrum and lightcurve of XTE J1550-564.

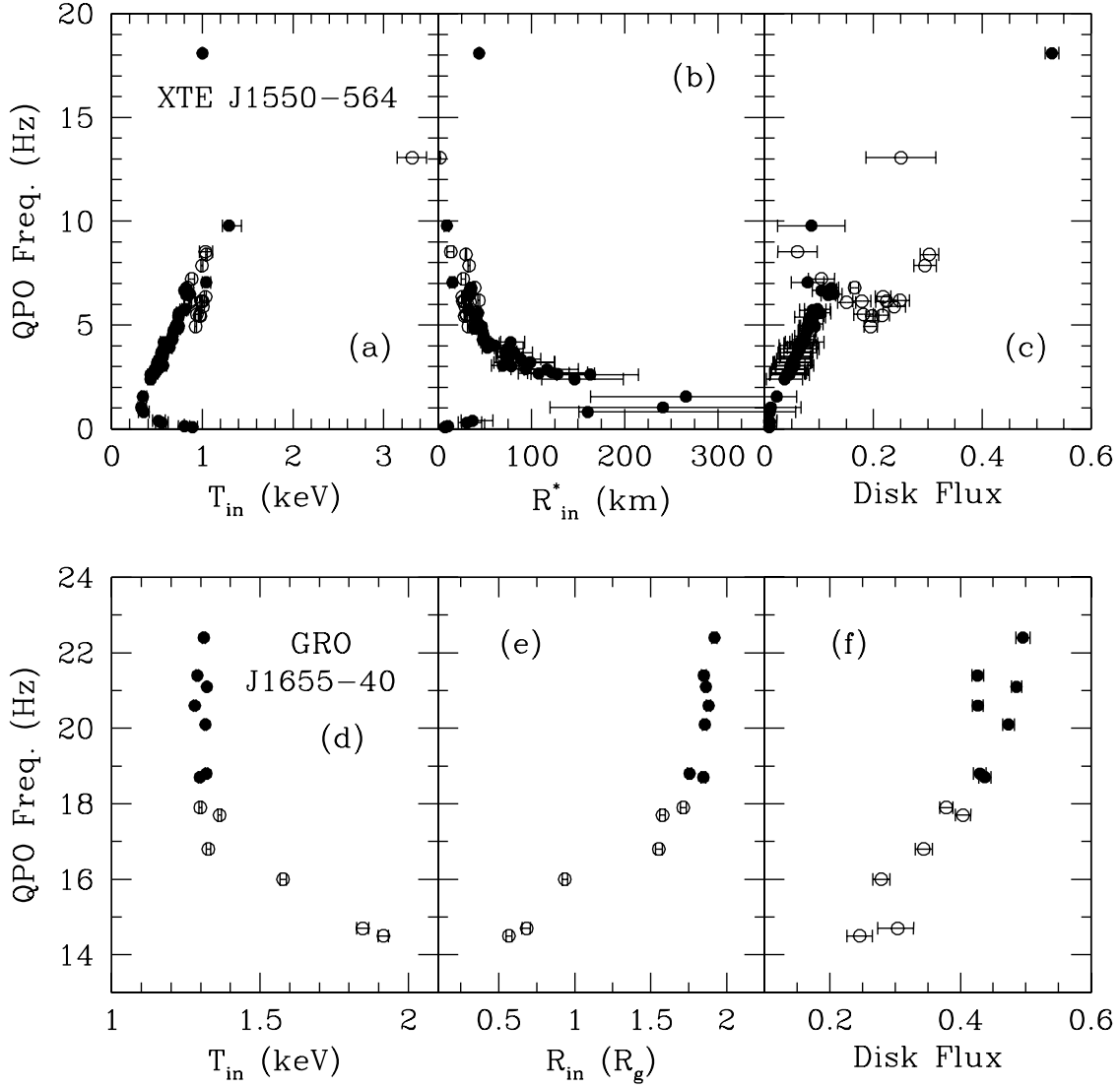


Fig. 2.— QPO frequency vs. Disk Parameters and Flux for the variable frequency 0.08–22 Hz QPOs in (a-c) XTE J1550–564 and (d-f) GRO J1655–40. The quantities plotted here are the color temperature of the accretion disk ( $T_{in}$ ) in keV, the inner disk radius ( $R_{in}$ ), and the unabsorbed 2–20 keV disk flux in units of  $10^{-7}$  erg s $^{-1}$  cm $^{-2}$ . For XTE J1550–564,  $R_{in}^* = R_{in}(\cos i)^{1/2}/(D/6 \text{ kpc})$  in km, where  $i$  is the inclination angle and  $D$  is the distance to the source in kpc. For GRO J1655–40,  $R_{in}$  is in units of  $GM/c^2 = 10.4$  km, where  $M = 7 M_{\odot}$ ,  $D = 3.2$  kpc (Hjellming & Rupen 1995), and  $i = 69^{\circ}.5$  (Orosz & Bailyn 1997). The open symbols represent observations in which a high-frequency (161–300 Hz) QPO is also observed. When error bars are not visible, it is because they are comparable to or smaller than the plotting symbol.

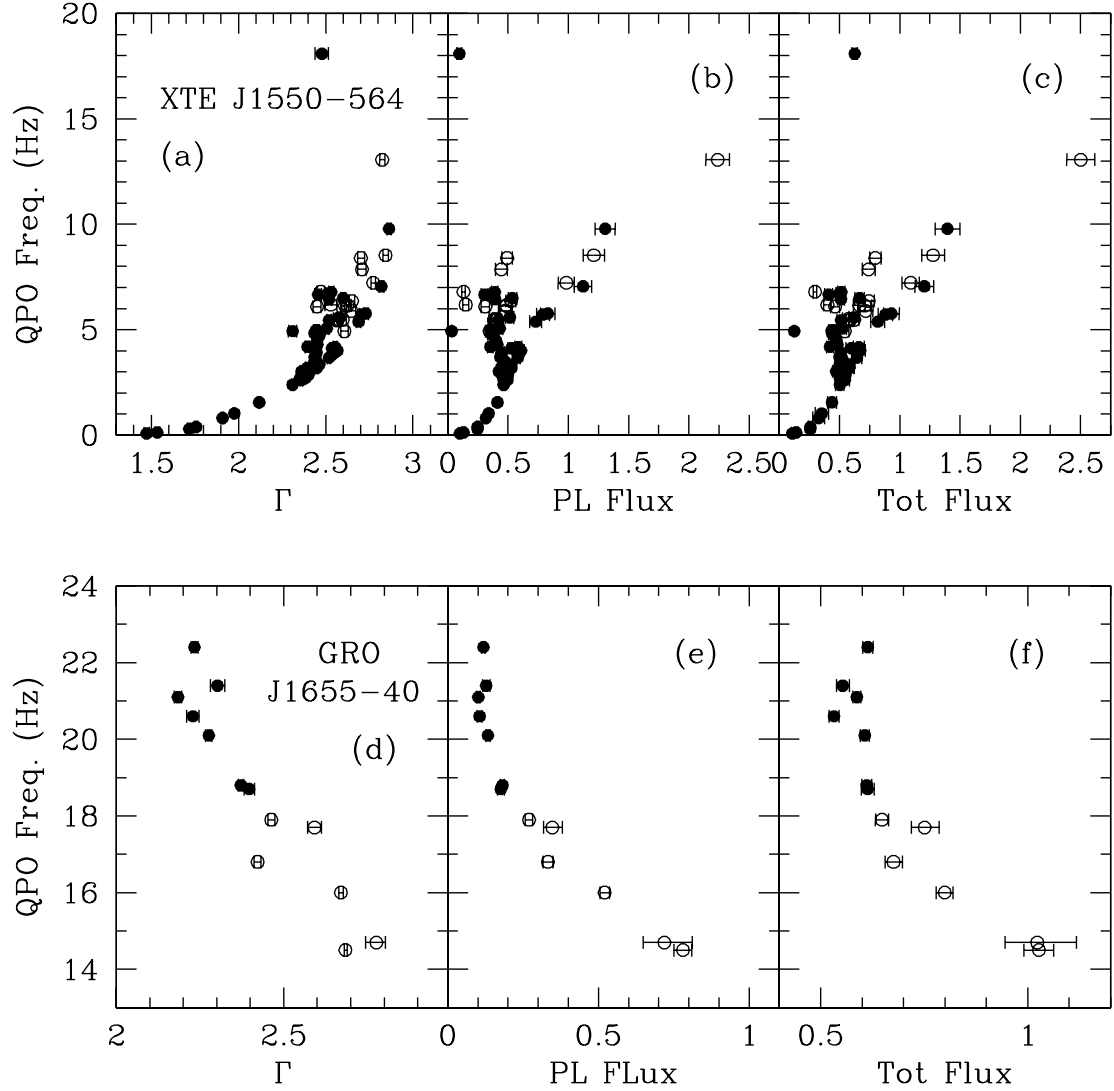


Fig. 3.— QPO frequency vs. Power-law Parameters and Total Flux for the variable frequency 0.08–22 Hz QPOs in (a-c) XTE J1550–564 and (d-f) GRO J1655–40. The quantities plotted here are the power-law photon index  $\Gamma$  and the unabsorbed 2–20 keV power-law and total fluxes in units of  $10^{-7}$  erg s $^{-1}$  cm $^{-2}$ .

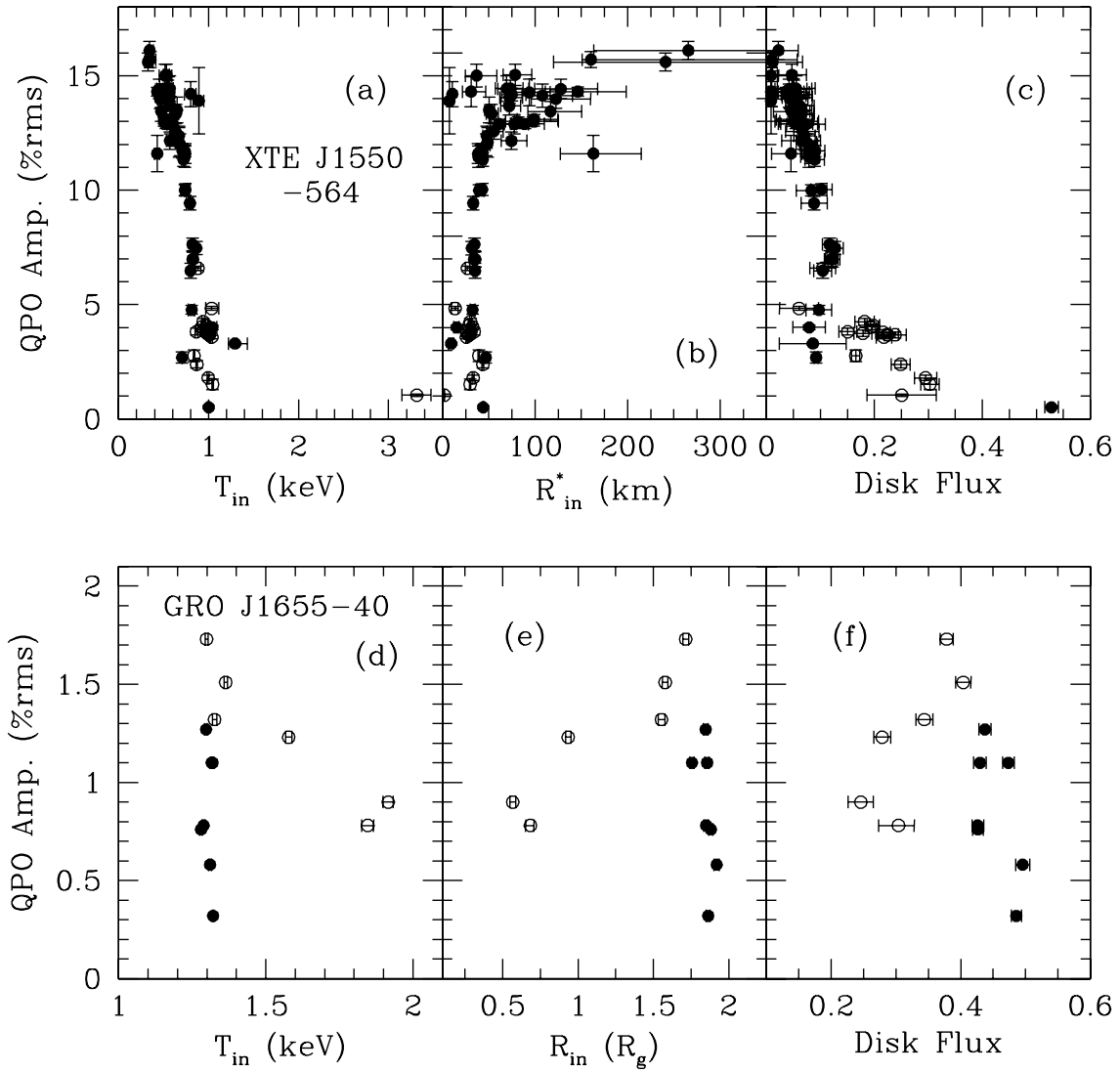


Fig. 4.— QPO Integrated Fractional RMS Amplitude vs. Disk Parameters and Flux for the variable frequency 0.08–22 Hz QPOs in (a-c) XTE J1550–564 and (d-f) GRO J1655–40.

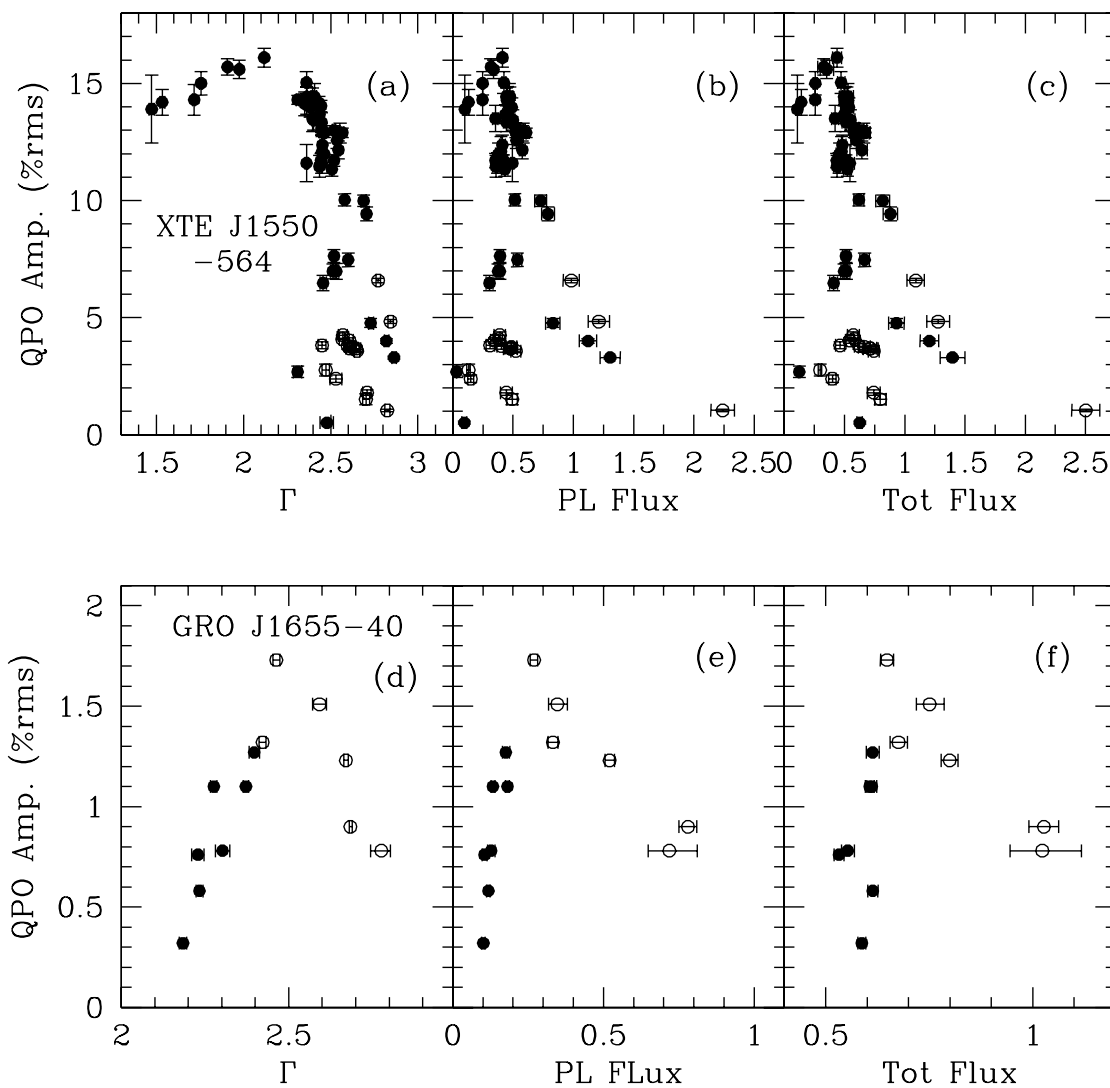


Fig. 5.— QPO Integrated Fractional RMS Amplitude vs. Power-law Parameters and Total Flux for the variable frequency 0.08–22 Hz QPOs in (a-c) XTE J1550–564 and (d-f) GRO J1655–40.

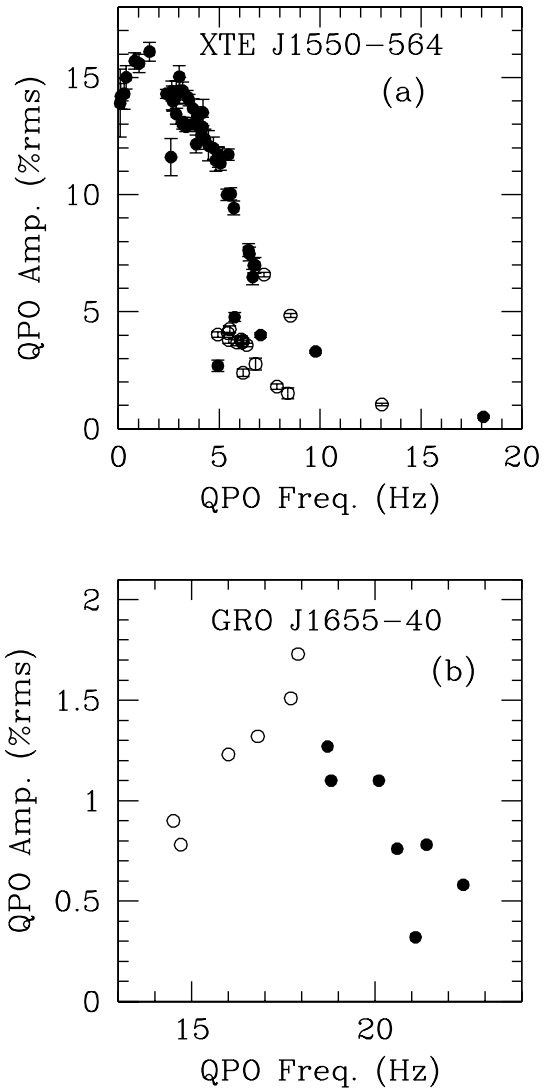


Fig. 6.— QPO Integrated Fractional RMS Amplitude vs. Frequency for the variable frequency 0.08–22 Hz QPOs in (a) XTE J1550–564 and (b) GRO J1655–40.

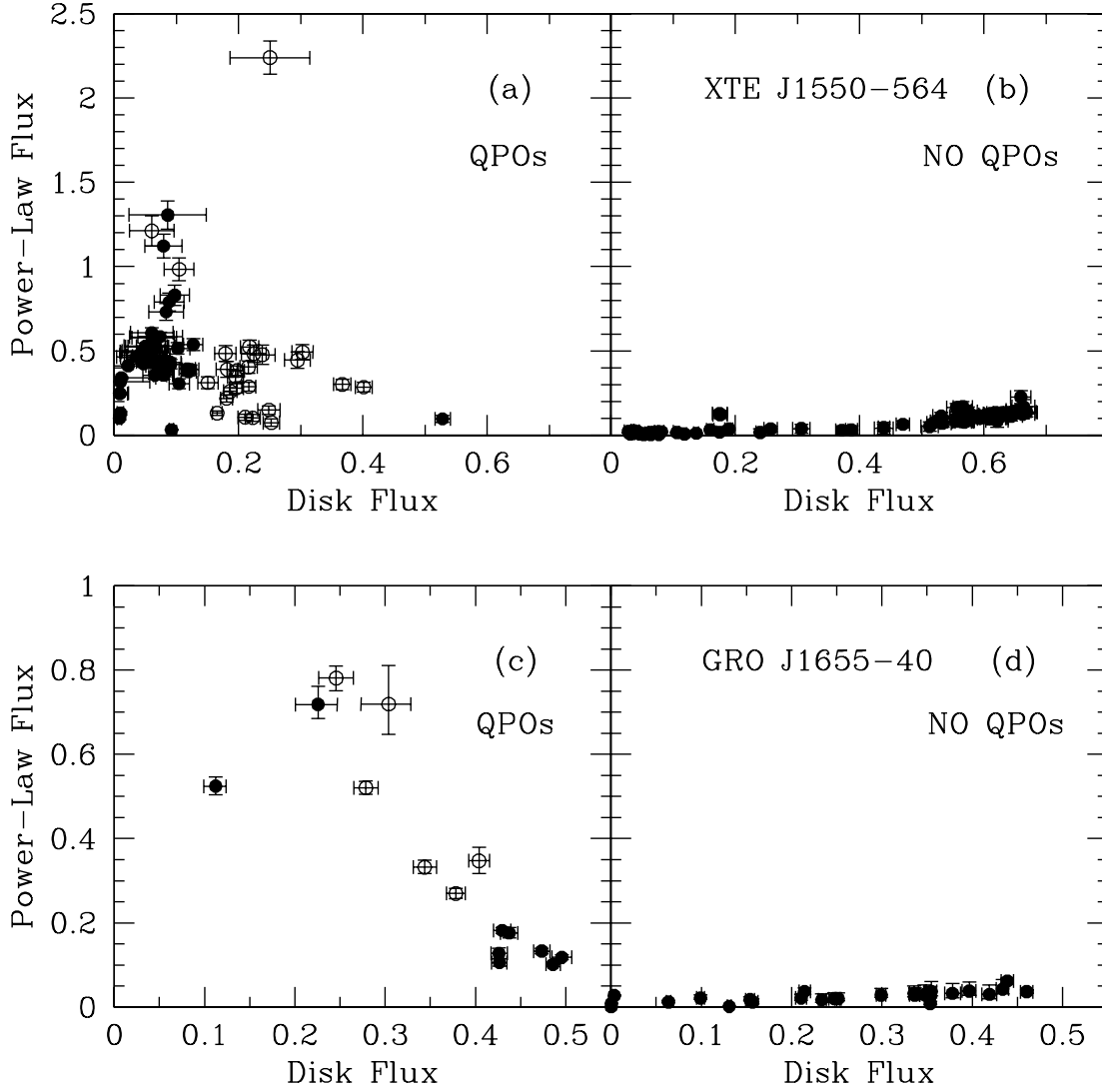


Fig. 7.— Power-Law Flux vs. Disk Flux for (a,b) XTE J1550-564 and (c,d) GRO J1655-40 when the QPOs are present (a,c) and absent (b,d). Flux is in units of  $10^{-7}$  erg  $s^{-1}$   $cm^{-2}$ . The open symbols represent observations in which a high-frequency (161-300 Hz) QPO is also observed. The two data points in (c) at high power-law flux for which no high-frequency QPOs are observed are not included in the previous figures or the discussion of variable frequency QPOs because this QPO near 10 Hz is present in 12 observations with an approximately constant frequency.